Satellite-based InSAR: application and signal extraction for the detection of landslide precursors

BENEDETTA DINI[1], MARIE-PIERRE DOIN[1], PASCAL LACROIX[1], MICHEL GAY[2]

[1] ISTerre, Université Grenoble-Alpes
1381 Rue de la Piscine, 38610, Gières, France
[2] GIPSA-Lab
11 Rue des Mathematiques, 38400, Saint-Martin-d'Hères, France

benedetta.dini@univ-grenoble-alpes.fr, marie-pierre.doin@univ-grenoble-alpes.fr,
pascal.lacroix@univ-grenoble-alpes.fr, michel.gay@gipsa-lab.grenoble-inp.fr

1 Introduction

One of the major open questions in the domain of landslide hazard assessment and prediction is related to the timely and accurate detection of precursors, key indicators that precede failure or phases of large accelerations. Whilst in situ-methods, be these geotechnical, geodetic or geophysical, offer high level of accuracy at point locations or over restricted areas, they are often very costly in terms of instrumentation and manpower. Moreover, installation of in-situ networks requires previous knowledge of an instability. Therefore, despite the high accuracy they can achieve they do not contribute to the ability to detect previously unknown landslides that might be undergoing phases of destabilisation.

In the last few decades, the increasing availability of satellite-based SAR imagery, characterised by large coverages and increasing temporal sampling, has allowed scientists to use InSAR techniques exploiting phase difference between successive images to identify previously unknown gravitational instabilities over inaccessible areas[1], and to accurately quantify displacements[2–4].
In some cases, retrospective retrieval of time series revealed acceleration patterns precursory to failure[5–7]. This suggests that, the higher temporal sampling of new generation satellites, may indeed offer in the future the opportunity to detect motion precursory to failure with viable lead time for warning.

However, the full potential of satellite based InSAR has not yet been realised for monitoring slope movements, owing to signal loss and a decrease in resolution caused by high noise levels due to vegetation, by high phase gradients due to large displacements over restricted areas, by unfavourable orientation and by the limitations of standard unwrapping procedures used to convert the wrapped measurement (radians) into displacements (mm)[8,9]. In addition, the incipient stages of deformation are rarely detected because they commonly develop over areas equivalent to a few pixels, challenging signal extraction with current available resolution.

We show a methodology to retrieve signal associated with key precursors of destabilisation for landslides that present characteristics unfavourable to unwrapping and to time series inversion methods. This methodology entails detailed analysis and description of the interferometric phase signal obtained from raw, wrapped interferograms in combination with the analysis of interferometric coherence drops as marker for key geomorphological features.

2 Methodology

We generated 471 Sentinel-1 wrapped interferograms, covering the period between April 2015 and March 2022, at medium spatial resolution (8 and 2 looks in range and azimuth respectively, for a pixel of roughly 18 along range by 31 m in azimuth) over the Colca Valley in Peru. The interferograms were produced with the NSBAS processing chain, and the topographic contribution of the signal was removed with the SRTM digital elevation model (30 m resolution). Since landslides behaviour is often highly non-linear and is characterised by phases of quiescence and reactivation, for each investigated landslide we selected interferograms with short and constant temporal baseline. This is to ensure that the signal observed at each time step would not be affected by the length of time elapsed between the images used to form an interferogram. Various temporal baselines were tested: 12, 24 and 36 days, for which 124, 139 and 120 interferograms are available, respectively. We observed that, for the landslide characteristics, vegetation, topography and rainfall in this study and with the wavelength of Sentinel-1, the shortest available temporal baselines (12 and 24 days) allow for an overall higher signal to noise ratio than longer ones. For each of the investigated landslides we visually mapped the landslide boundaries based on

geomorphological characteristics in geographical coordinates on optical images (Google Earth or Planet Lab imagery). We then projected the polygon outline in the geometry of the radar images and then performed a crop of all interferograms around the landslide polygon.

The size of the crop is selected in order to have a margin around the landslide of about the same size of the landslide. This allows a good size for the analysis as well as the presence of areas assumed stable and characterised by good temporal interferometric coherence (above 0.4) outside the landslide for reference. Interferometric coherence, γ, is calculated over a 5 x 5 pixels window during the interferogram generation. It is calculated as:

$$\gamma = \frac{|\langle S_1 \cdot S_2^* \rangle|}{\sqrt{\langle S_1 \cdot S_1^* \rangle \langle S_2 \cdot S_2^* \rangle}} \; (1)$$

where $\langle \cdot \rangle$ indicates the averaging of the complex conjugation over the chosen window and S_1 and S_2 are the complex values of two images composing an interferogram[10].

In the following sections, we illustrate the removal from the raw interferograms of a component of the phase signal proportional to perpendicular baselines, the analysis of the evolution of the phase signal in time and of coherence loss patterns.

2.1   Topographic error correction of raw interferograms

For each case analysed, an area assumed stable (not affected by ground displacements) was chosen outside the landslide boundaries. Different window sizes were tested and we selected a 5 x 5 pixels window: this is large enough to obtain more meaningful complex average phase values than for an individual pixel, whilst small enough not to include areas with too different reflective properties. The choice of the window was based on visual geomorphological analysis of the area surrounding the landslide as well as average temporal coherence, as a proxy for phase stability. The phase of each raw, wrapped interferogram was referenced to the average phase of the chosen stable reference window, $e^{i\varphi_{k,ref}}$, computed for each interferogram, k.

We then investigated the effect of the perpendicular baselines of each interferogram on the phase. Higher perpendicular baselines cause higher sensitivity to topography, therefore if topographic residuals exist after the topographic component removal with the SRTM DTM, a correlation with the interferometric phase would be revealed. To do this, we computed the average phase the 5 x 5 pixels moving window, l, over the entire crop, noted $e^{i\delta\varphi_{k,l}}$. We then investigated for each window the relationship between interferometric phase and perpendicular baseline for the whole temporal series of
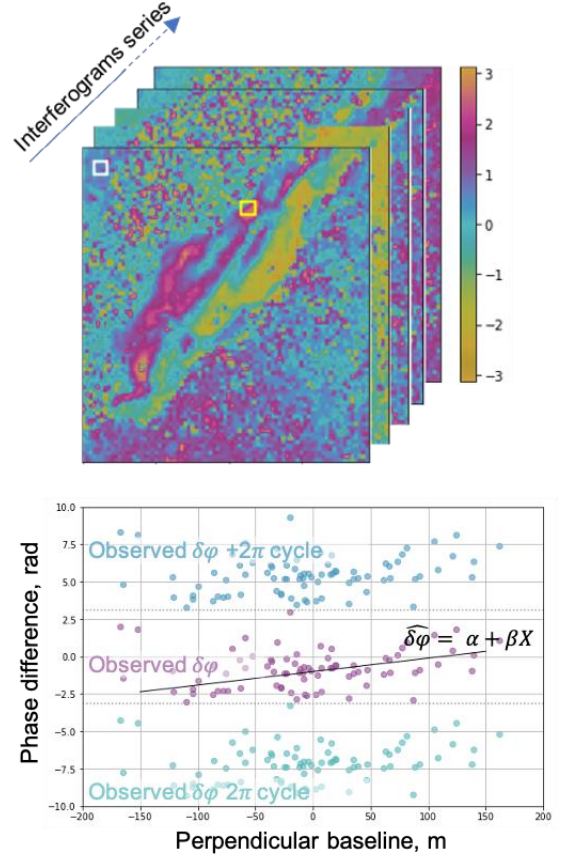

Figure 1. Example of correlation between phase and perpendicular baseline for a window shown in the yellow square. Each purple point represents the complex average phase in the yellow window for a given interferogram of the series with respect to the complex average phase in the reference area (white square). As the phase is known in modulo 2π, its $+2\pi$ and -2π values are also shown in blue and teal respectively.

interferograms. This was done by performing a parameter search to find the best linear fit in the complex realm, to account for the circularity of the phase values, as the interferograms are wrapped. For each moving window, l, and for each interferogram, k, predicted values were calculated as:

$$e^{i\widehat{\delta\varphi}_{k,l}} = e^{iX_k\beta_l} \; (2)$$

where $e^{i\widehat{\delta\varphi}_{k,l}}$ is the predicted phase in each window l, X_k is the perpendicular baseline of each interferogram and β_l is the proportionality coefficient between $e^{i\delta\varphi_{k,l}}$ and perpendicular baseline for the window l (Fig. 1). For the parameter search, several bounds were tested for β before choosing -0.5 and 0.5 rad/m, with a 0.001 step. A value of β is obtained by maximising the coherence between the predicted and the observed values:

$$\rho_k = \left| \sum_k e^{i\varphi_{k,l}} * e^{i\widehat{\delta\varphi_{k,l}}^*} / N \right| \; (3)$$

where N is the number of interferograms (Fig. 1). Maps of β, ρ and corrected interferograms were then obtained (Fig. 2).
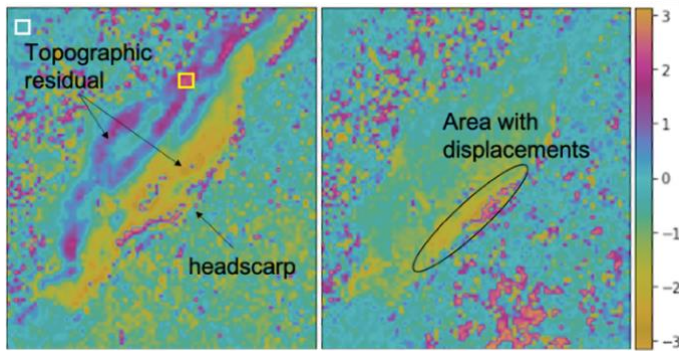
Figure 2. Example of correction for the effect of perpendicular baseline. Left, raw interferogram; right, corrected interferogram.

2.2 Phase difference

After interferogram correction, time series of wrapped phase difference between the stable area and an area at the crown of the landslide were investigated, after referencing to the reference area. Precursors are expected to be observed in the upper part of the landslide, in an area where headscarp retrogression might occur in subsequent destabilisation phases. The changes of phase difference through time between the stable area and an area where retrogression might occur should thus be a proxy for acceleration of displacement rates. In order to limit the effect of the noise of the interferometric phase within the landslide boundaries, we performed a selection of a 3 by 3 pixels window, based on average temporal coherence. Although it was not possible to select a specific threshold for temporal coherence, given the large variability, the selection of the area was based on the necessity to target the crown of the landslide whilst retaining the highest relative temporal coherence. Several window sizes were tested, and the size above was chosen. However, different window sizes could be chosen, depending on specific characteristics. Phase differences time series are initially assigned a degree of reliability associated with a visual inspection of all interferograms. Moreover, each point in the time series is assigned a quantitative measure of uncertainty which relates to the departure from a second degree polynomial to the correlation between phase standard deviation and average coherence within the reference and target windows.

2.3 Coherence drop patterns

We investigated spatial patterns of interferometric coherence loss both within the landslide and in the surrounding area. Coherence loss patterns that occur over restricted areas are considered a proxy of localised strain, as localised changes of the complex interferometric values are likely associated with localised displacements. The spatial analysis of coherence loss is carried out over individual interferograms. We calculated for interferogram the average coherence over three areas: the whole crop, the mapped landslide boundaries and a polygon defining the crown and scarp of the landslide (the latter mapped on optical images on the basis of geomorphological analysis, as for the landslide boundaries). We then analyse the average coherence time series in relation to daily rainfall (from the national service of Meteorology and Hydrology of Peru). We computed the time series of the ratio of average landslide coherence over the average coherence of the whole area considered.

3 Results

We show two examples of investigated landslides. These are large (between 0.8 and 1 km along the headscarp) deep-seated landslides in the Colca Valley. One of these landslides previously unidentified, failed on 18th June 2020, causing river damming. On this landslide we observe changes of the phase difference of roughly 2.5 radians between the stable reference area and the target area at the crown, in the weeks prior to the failure. This is likely associated with an acceleration of the downslope displacements.

Seasonal coherence loss is seen both within the landslide and in the surrounding area, in correspondence with wet periods over the years preceding the failure. However, we also observe significant, local coherence loss along the scarp and the southeastern flank of the landslide, intermittently in the years before failure, in periods in which coherence was overall higher in the surrounding area. Such coherence loss patterns appear in localised, elongated areas which mark prior to failure the developing headscarp (Fig. 3A). Optical images do not allow to recognise such feature as it develops. This observation is accompanied by a sharp decrease in the ratio between the coherence within the landslide and in the surrounding area, from 1 to 0.25, roughly six months before the failure. This could be associated with irreversible and gradual deformation on the ground related to internal damage of the structure of the landslide material.

The second landslide analysed in this work has not yet undergone catastrophic failure but it has been characterised by periods of high velocities of displacements, reaching around 12 m of downslope displacement in 2020. From early 2017, the interferometric coherence maps indicate the formation of a head scarp and of multiple secondary scarps over the body of the landslide (Fig 3B). We observe that the coherence drops that mark the boundaries of important morphological features appear to occur with different timings, which might reflect the activation of parts of the landslides in stages. This might have implication in the understanding of the different response to trigger of
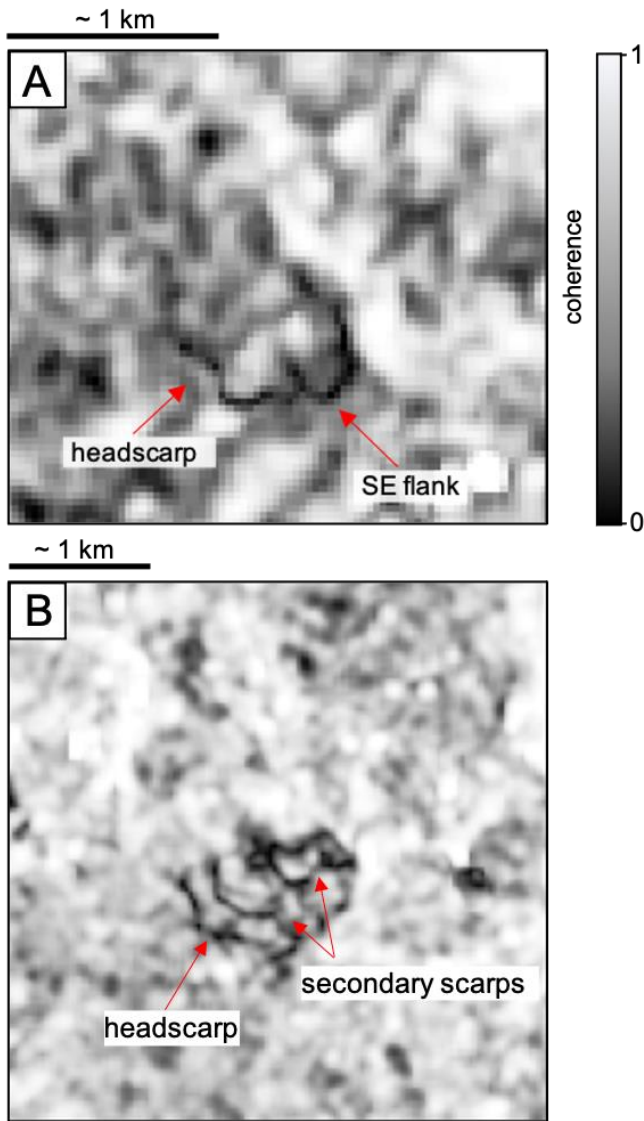
Figure 3. Examples of interferometric coherence loss pattern observed for A) one of the investigated landslides in the period 27/11/2017 – 9/12/2017, marking the southeastern flank and headscarp of the landslide two and a half years prior to failure; B) another landslide in the same valley showing the formation of multiple scarps, likely separating sectors of activity.

various sectors of the landslide through time. It also indicates that the landslide might be approaching a phase of rapid destabilisation.

4 Conclusions

This type of approach is promising with respect to the extraction of relevant information from interferometric data when the generation of accurate and continuous time series of displacements is hindered by the nature of landcover or of the landslide behaviour, such in the cases of the landslides presented here. The combination of key, relevant parameters and their changes through time obtained with this methodology may prove necessary for the identification of precursors over a wider range of landslides than with time series generation alone.

Moreover, the accurate description of such precursors for a wider pool of cases will also allow for the extraction of spatial patterns of coherence loss over large areas, also

with the aid of machine learning methods. In this way, it would become possible to identify destabilising, possibly unknown landslides over large areas and then focus the analysis with the method described above on specific slopes.

The methodology discussed here is necessary in order to make a step change in the use of satellite imagery for early warning of landslide failure. We show its use with Sentinel-1 data (C-band), but it will become increasingly relevant with the launch of satellites carrying L-band SAR sensors, with frequent repeat pass.

References
1. Dini, B., Manconi, A. & Loew, S. Investigation of slope instabilities in NW Bhutan as derived from systematic DInSAR analyses. *Eng. Geol.* **259**, (2019).
2. Wasowski, J. & Bovenga, F. Investigating landslides and unstable slopes with satellite Multi Temporal Interferometry: Current issues and future perspectives. *Eng. Geol.* **174**, 103–138 (2014).
3. Liu, P. *et al.* Using advanced InSAR time series techniques to monitor landslide movements in Badong of the Three Gorges region, China. *Int. J. Appl. Earth Obs. Geoinf.* **21**, 253–264 (2013).
4. Dini, B., Manconi, A., Loew, S. & Chophel, J. The Punatsangchhu-I dam landslide illuminated by InSAR multitemporal analyses. *Sci. Rep.* **10**, 1–10 (2020).
5. Intrieri, E. *et al.* The Maoxian landslide as seen from space: detecting precursors of failure with Sentinel-1 data. *Landslides* **15**, 123–133 (2018).
6. Carlà, T. *et al.* Author Correction: Perspectives on the prediction of catastrophic slope failures from satellite InSAR (Scientific Reports, (2019), 9, 1, (14137), 10.1038/s41598-019-50792-y). *Sci. Rep.* **9**, 1–9 (2019).
7. Dong, J. *et al.* Measuring precursory movements of the recent Xinmo landslide in Mao County, China with Sentinel-1 and ALOS-2 PALSAR-2 datasets. *Landslides* **15**, 135–144 (2018).
8. Lacroix, P., Dini, B. & Cheaib, A. Measuring kinematics of slow-moving landslides from satellite images. in *Displacement measurement by remote sensing Imagery* (2021).
9. Werner, C., Wegmüller, U., Strozzi, T. & Wiesmann, A. Processing strategies for phase unwrapping for INSAR applications. in *Proceedings of the European Conference on Synthetic Aperture Radar EUSAR* (2002).
10. Kumar, V. & Venkataraman, G. SAR interferometric coherence analysis for snow cover mapping in the western Himalayan region. *Int. J. Digit. Earth* **4**, 78–90 (2011).